JOURNAL OF MAGNETIC RESONANCE **86,** 470–487 (1990)

Dynamic-Angle Spinning of Quadrupolar Nuclei

K. T. MUELLER, B. Q. SUN, G. C. CHINGAS, J. W. ZWANZIGER,
T. TERAO,* AND A. PINES

Lawrence Berkeley Laboratory and Chemistry Department,
University of California, Berkeley, California 94720

Received May 16, 1989; revised July 15, 1989

In dynamic-angle spinning (DAS), a sample spins around an axis inclined at an angle $\theta(t)$ with respect to the magnetic field such that the averages of $P_n(\cos\theta)$ are zero. The simplest case is where $\theta(t)$ assumes two discrete values θ_1 and θ_2 (complementary DAS angles) such that the averages of $P_2(\cos\theta)$ and $P_4(\cos\theta)$ are zero, thereby removing second-order quadrupolar (and dipolar) broadening. Examples of DAS complementary angles are $\theta_1 = 37.38°$ and $\theta_2 = 79.19°$. Experimental details for DAS experiments are provided and applications to sodium-23 and oxygen-17 NMR illustrate the enhanced resolution achieved by removing the second-order broadening inherent in magic-angle spinning.

The NMR technique of magic-angle spinning (MAS) (*1–3*) spatially averages anisotropic interactions such as chemical shifts, yielding high-resolution spectra of many spin-$\frac{1}{2}$ nuclei in solids (*4, 5*). Additional broadening arising from dipolar interactions can be dealt with by spin decoupling and multiple-pulse sequences (*6*). In contrast to the case of spin-$\frac{1}{2}$, quadrupolar nuclei in solids may experience large anisotropic interactions with local electric field gradients, which are not completely averaged away by MAS. Of particular interest in high-field NMR is the central ($\frac{1}{2} \leftrightarrow -\frac{1}{2}$) transition in nuclei with half-integer spin angular momentum greater than one. The central transition is not affected by first-order quadrupolar interactions, but there is a shift and broadening due to second-order effects, as illustrated for spin-$\frac{3}{2}$ in Fig. 1. It is the second-order broadening that limits the resolution for important nuclei such as boron-11, oxygen-17, sodium-23, and aluminum-27.

The perturbation of the central transition resonance frequency in quadrupolar nuclei has both isotropic and anisotropic components. When averaged over the orientations of the crystallites in a polycrystalline sample the isotropic term is manifested as a shift of the center of gravity of the resonance, and the anisotropy gives rise to a broad, asymmetric lineshape (*7, 8*). The anisotropic contribution is partially aver-

* Permanent Address: Department of Chemistry, Kyoto University, Faculty of Science, Kyoto 606, Japan.

0022-2364/90 $3.00

DOI of original item: doi: 10.1016/0022-2364(90)90025-5

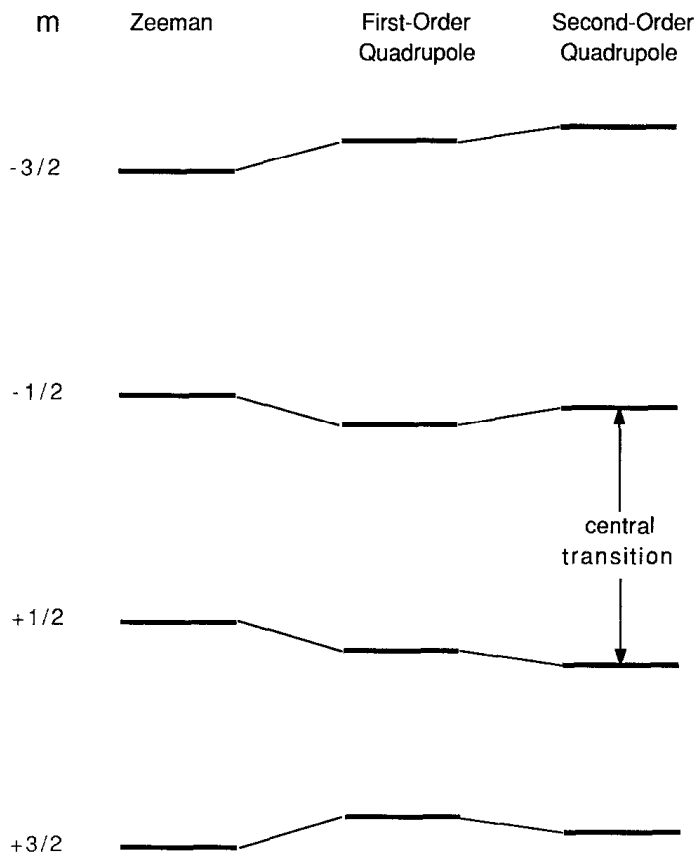

FIG. 1. First- and second-order frequency shifts of the Zeeman levels of a spin-$\frac{3}{2}$ nucleus due to the interaction of the nuclear quadrupole moment with the local electric field gradient in a crystallite. The central transition is not effected by the first-order effects, but is shifted in second-order leading to a broad line when summed over all orientations of crystallites in a powdered sample.

aged by MAS (*9, 10*) or by spinning at angles other than the magic angle (*11*), but the line remains broad in comparison to the results from spin-$\frac{1}{2}$ nuclei.

An example of second-order quadrupolar broadening is shown in Fig. 2, where the static spectrum observed for the central transition of the sodium-23 ($I = \frac{3}{2}$) resonance in polycrystalline sodium oxalate ($Na_2C_2O_4$) has a width of approximately 13 kHz. Under MAS the line narrows, with a residual second-order linewidth on the order of 4 kHz as shown at the bottom in Fig. 2. Since there is only one distinct type of sodium site and no overlapping resonances, the quadrupolar parameters are easily obtained by computer simulation, yielding $e^2qQ/h = 2.5$ MHz and $\eta = 0.7$ for the quadrupolar coupling constant and asymmetry parameter, respectively. In the case where there are several similar sites in a sample, overlapping patterns in both the static and the spinning spectra make such an analysis difficult.

Since the second-order interaction is inversely proportional to the static magnetic field strength, resolution can be increased by working in higher magnetic fields (*12*), but in some cases fields in excess of 25 T might be necessary. An alternative solution is to average the higher-order effects by removing the constraint of spinning about a

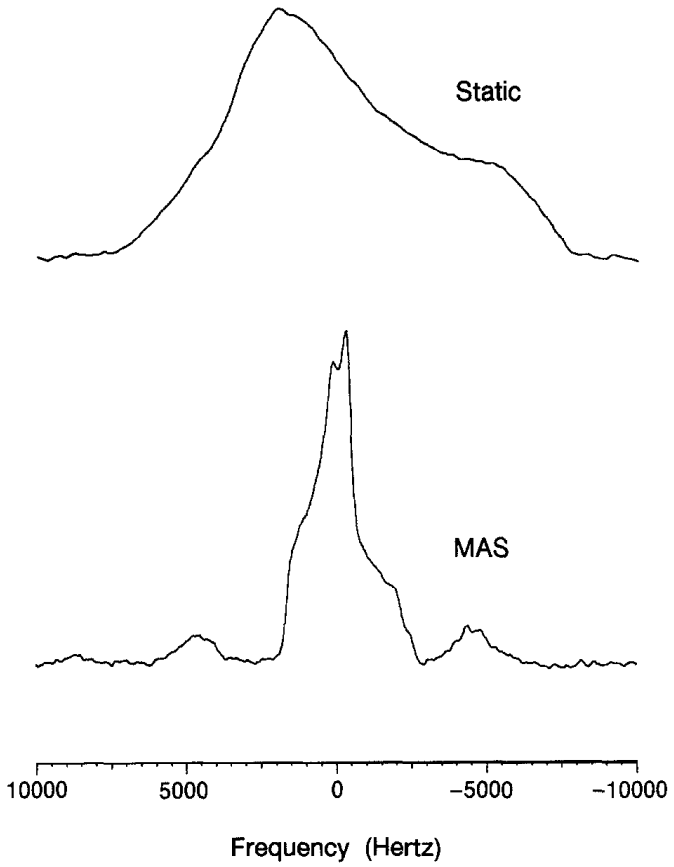

FIG. 2. Static and magic-angle spinning (MAS) spectra of the central transition for the sodium-23 resonance in polycrystalline sodium oxalate. The static spectrum shows a second-order powder pattern caused by quadrupolar interactions, further broadened by homonuclear dipole–dipole couplings and chemical-shift anisotropy. In the MAS spectrum, spinning sidebands appear at the rotor frequency, ν_{rot} = 4.5 kHz, and the resonance is narrowed by a factor of approximately three.

single axis. Indeed, in recently proposed techniques (*13–15*) the spinner axis undergoes a time-dependent trajectory with respect to the external magnetic field. Double rotation (DOR) involves continuously moving the axis of a rotor in a cone, whereas dynamic-angle spinning (DAS) employs evolution at discrete orientations of the spinner axis (*16, 17*). Preliminary results have demonstrated the promise of both DOR and DAS for oxygen-17 in solids (*18*).

In this paper we expand upon the DAS results of Ref. (*18*), including a brief discussion of the necessary theory and some details about experimental design and implementation. Experimental results from sodium-23 and oxygen-17 nuclei in inorganic solids illustrate the averaging of second-order quadrupolar interactions in both one- and two-dimensional NMR experiments.

BRIEF REVIEW OF DAS

Consider a spin Hamiltonian consisting of Zeeman and quadrupolar terms in high magnetic field:

$$\mathscr{H} = \mathscr{H}_Z + \mathscr{H}_Q. \quad [1]$$

The isotropic chemical shift is included in the Zeeman term,

$$\mathscr{H}_Z = -\gamma(1 - \sigma_{iso})B_0 I_Z = \omega_L I_Z, \quad [2]$$

where ω_L is the Larmor frequency.

In an interaction picture rotating about the laboratory z axis at ω_L, the quadrupolar Hamiltonian is rendered time dependent, and coherent averaging theory (*19, 20*) is utilized to obtain corrections to the Zeeman energy levels. The first-order corrections to the transition frequencies are calculated by averaging the interaction Hamiltonian over one Larmor period. For a spin with a principal axis system (PAS) related to the laboratory axis system by the Euler angles (α, β, γ), the correction to the transition frequency between the m and $m-1$ Zeeman levels is

$$\omega^{(1)}_{m\leftrightarrow m-1} = (m - \tfrac{1}{2})\omega_Q[\tfrac{3}{2}\cos^2\beta - \tfrac{1}{2} - \tfrac{1}{2}\eta \sin^2\beta \cos 2\alpha], \quad [3]$$

where

$$\omega_Q = \frac{3e^2qQ}{2I(2I-1)\hbar} \quad [4]$$

and η is the asymmetry parameter for the quadrupolar interaction.

For $m \neq \frac{1}{2}$ the transition frequencies for the crystallites in a powder are often distributed over a large range of values, making the resonance broad and difficult to detect. Using radiofrequency pulse amplitudes much less than the quadrupolar frequencies, we may restrict our attention to the central $(\frac{1}{2} \leftrightarrow -\frac{1}{2})$ transition, which is not broadened or shifted by first-order effects. The next approximation, involving the commutators of the time-dependent quadrupolar Hamiltonian with itself at different times, may be calculated analytically (*10*). The result is a second-order powder pattern which has distinct singularities and shoulders, as has also been calculated by a Rayleigh–Schrödinger perturbation theory approach (*21*).

Substantial line narrowing is accomplished by spinning a quadrupolar sample with an angular frequency ω_r at an angle θ with respect to the external magnetic field. In the limit that $\omega_r \ll \omega_Q \ll \omega_L$ the second-order contribution to the central transition frequency for an arbitrary crystallite is (*22, 23*)

$$\omega^{(2)}_{1/2\leftrightarrow -1/2} = \omega^{(2)}_{iso} + \sum_{l=2,4} A_l(\alpha', \beta')P_l(\cos\theta). \quad [5]$$

The isotropic shift due to second-order quadrupolar effects is

$$\omega^{(2)}_{iso} = -\frac{1}{30}\frac{\omega_Q^2}{\omega_L}\left[I(I+1) - \frac{3}{4}\right]\left(1 + \frac{1}{3}\eta^2\right). \quad [6]$$

The $A_l(\alpha', \beta')$ terms in Eq. [5] describe the anisotropic contributions, dependent on the Euler angles (α', β') describing the transformation between the quadrupolar PAS and the rotor axis system. The dependence on the rotor orientation with respect to the external field is given by the second- and fourth-order Legendre polynomials;

$$P_2(\cos\theta) = \tfrac{1}{2}(3\cos^2\theta - 1) \quad [7]$$

$$P_4(\cos\theta) = \tfrac{1}{8}(35\cos^4\theta - 30\cos^2\theta + 3), \quad [8]$$

which are sketched in the top part of Fig. 3.

Normal MAS amounts to setting $\theta = \theta^{(2)}$, where $P_2(\cos\theta^{(2)}) = 0$. Line narrowing of up to an order of magnitude may be obtained, but an anisotropic powder pattern remains due to the $P_4(\cos\theta)$ terms. Although angles $\theta^{(4)}$ exist where $P_4(\cos\theta^{(4)}) = 0$, there is no angle at which both $P_2(\cos\theta)$ and $P_4(\cos\theta)$ vanish.

An alternative to MAS is to make the angle θ time dependent by moving the spinning axis so that over the time of the experiment (T) the anisotropies are averaged away. Employing a distribution of angles described by the weight function $W(\theta)$, we require that for $l = 2$ *and* $l = 4$

$$\langle P_l(\cos\theta)\rangle = \int P_l(\cos\theta)W(\theta)d\theta = \int_0^T P_l(\cos\theta(t))dt = 0. \quad [9]$$

A number of solutions have been calculated, including "double rotation" and linear or cosinusoidal sweeps of the angle between two extremes, θ_1 and θ_2 (*13–15*). For a linear sweep possible solutions (θ_1, θ_2) are (19.05°, 99.19°) and (11.96°, 137.40°). A cosinusoidal sweep, where $\theta(t) = \theta_2 - (\theta_2 - \theta_1)\cos\alpha t$, has solutions (23.27°, 117.37°) and (27.38°, 90.10°). Double rotation corresponds to $\cos\theta(t) = \cos\theta^{(2)}\cos\theta^{(4)} + \sin\theta^{(2)}\sin\theta^{(4)}\cos\alpha t$; i.e., a spinner moves in a cone with half-apex angle $\theta^{(4)}$ ($\theta^{(2)}$) about the axis of another spinner inclined at $\theta^{(2)}$ ($\theta^{(4)}$) with respect to the external magnetic field. In DAS a set of N discrete angles are found such that

$$\sum_{i=1}^{N} P_2(\cos\theta_i)x_i = \sum_{i=1}^{N} P_4(\cos\theta_i)x_i = 0, \quad [10]$$

where x_i is the fraction of time spent at each angle. Consider now the minimal DAS solution, that is, when $N = 2$. Defining τ_i as the amount of time spent at each angle, and k as the ratio of the time spent at θ_2 to that spent at θ_1, or $k = \tau_2/\tau_1 = x_2/x_1$, there is an infinite number of solutions (θ_1, θ_2, k) such that

$$P_2(\cos\theta_1) = -kP_2(\cos\theta_2) \quad [11]$$

$$P_4(\cos\theta_1) = -kP_4(\cos\theta_2). \quad [12]$$

We call the sets of θ_1 and θ_2 pairs of *DAS complementary angles.* The valid solutions are shown graphically in Fig. 3, where the fraction of time spent at each of the two angles is found along the ordinates of the bottom graph.

Figure 4 shows simulated spectra for several pairs of complementary angles. For example, when $x_2 = x_1$, k is equal to unity and the solution is $\theta_1 = 37.38°$ and $\theta_2 = 79.19°$. Clearly, for each value of the parameter η the two spectra are mirror images about the isotropic shift. For values of k other than unity the spectra also appear as mirror images, now with a scaling factor k. For each spinning angle θ_i there is an isotropic and anisotropic frequency contribution for each crystallite. The isotropic shift, $\omega_{iso}^{(2)}$, is the same for every orientation of the quadrupolar PAS in the sample,

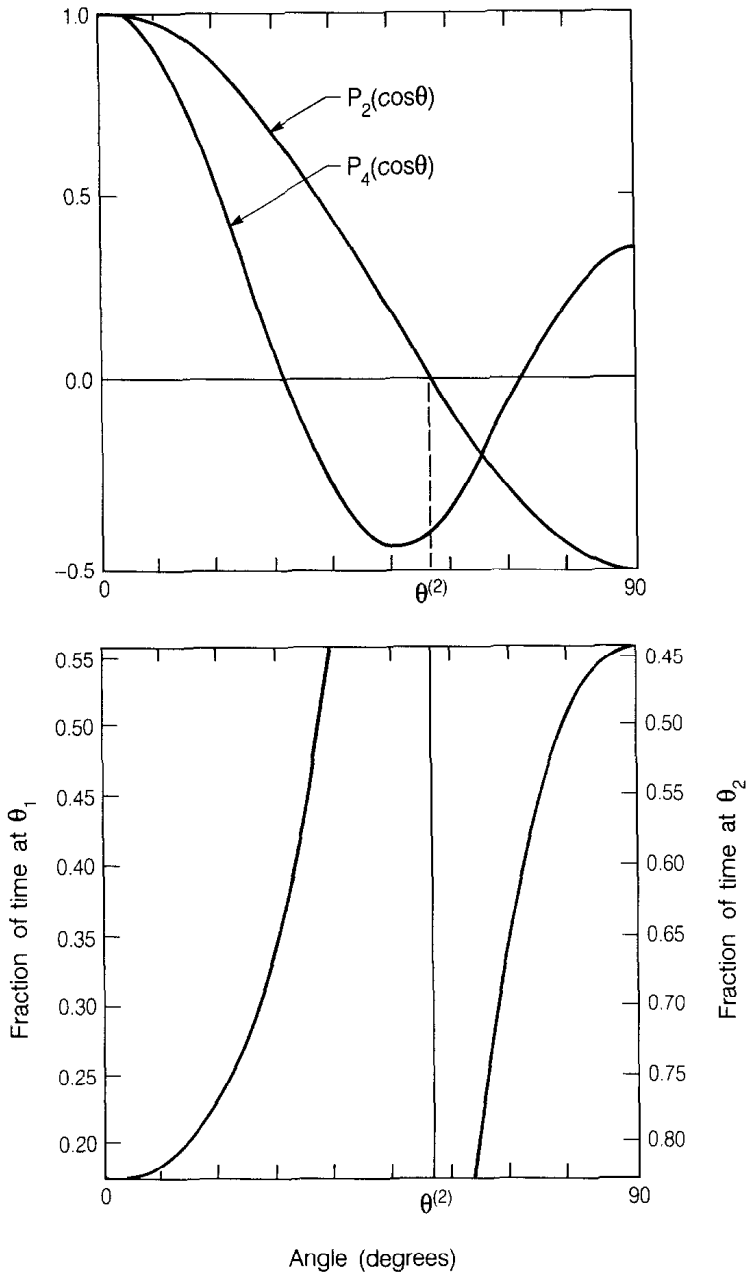

FIG. 3. Top: Functional forms of the second- and fourth-order Legendre polynomials (Eqs. [7] and [8]). The magic angle, $\theta^{(2)}$, is a root of the equation $P_2(\cos\theta^{(2)}) = 0$. Bottom: The solutions to Eqs. [11] and [12] presented graphically, with the corresponding fractions of the evolution time spent at each angle along the vertical angles. As an example, when $k = 1$ the fraction of time spent at each angle is 0.5, and the solutions are $\theta_1 = 37.38°$ and $\theta_2 = 79.19°$.

while the anisotropic term depends on both the crystallite orientation and the spinning angle θ_i, which we write $\omega_{\text{aniso},i}(\alpha', \beta', \theta_i)$. The two angles in a DAS experiment are chosen to be complementary, so that

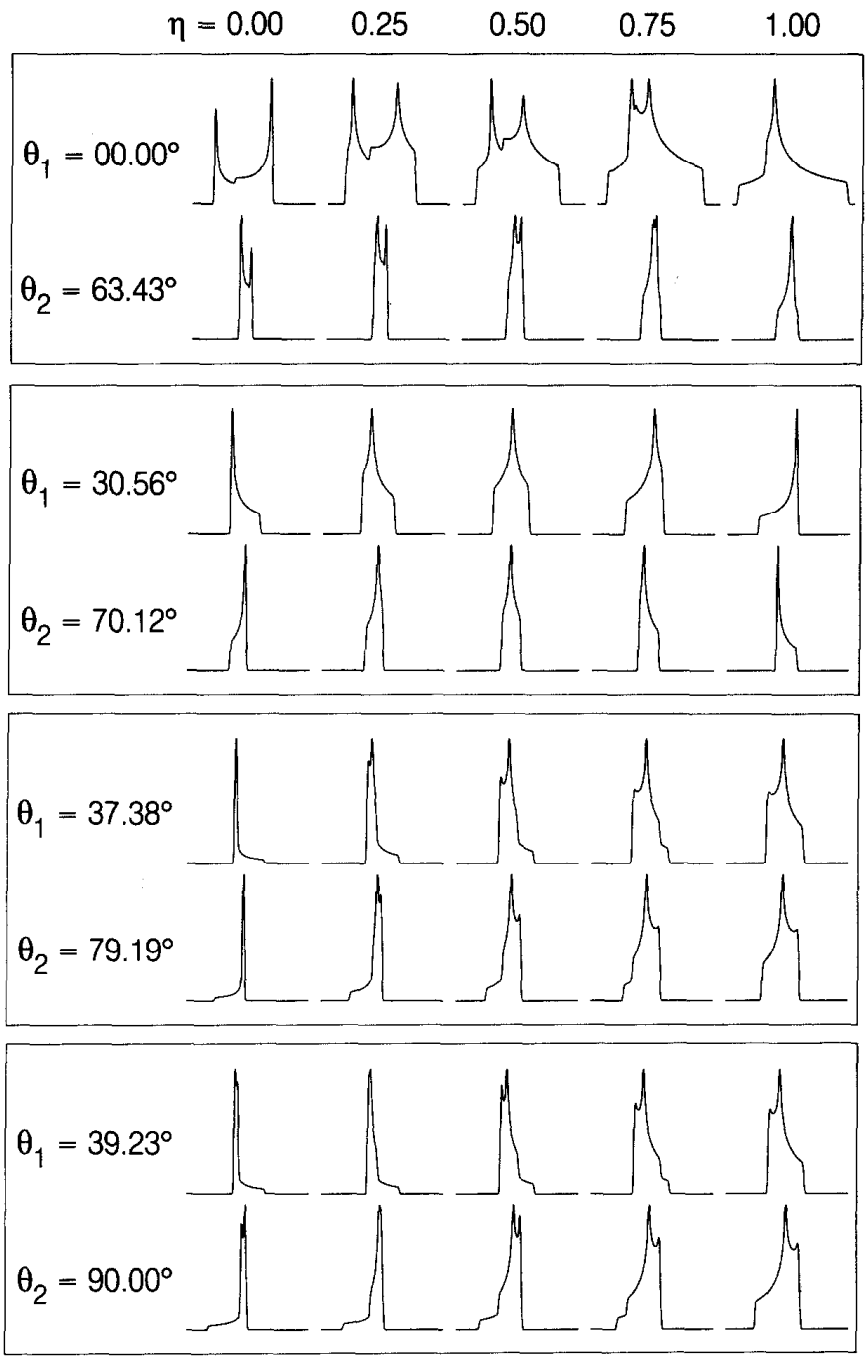

FIG. 4. Calculated second-order patterns obtained with rapid sample spinning for various values of the spinner axis angle and the asymmetry parameter (η) of the quadrupolar interaction. The paired angles are solutions to Eqs. [11] and [12] for various values of k. The first pair corresponds to the shortest time at θ_1 when $k = 5$. The second (the zeros of $P_4(\cos\theta)$) has $k = 1.87$, while the third is the experimentally demonstrated $k = 1$ case. The final pair, where the sensitivity of the experiment is a maximum for a coil moving with the sample, has $k = 0.8$.

$$\omega_{\text{aniso},1}(\alpha', \beta', \theta_1) = -k\omega_{\text{aniso},2}(\alpha', \beta', \theta_2), \quad [13]$$

and a DAS experiment is designed to cancel the anisotropic contributions for all crystallites in a sample. Of course DAS also averages the chemical-shift anisotropy.

A DAS experiment might therefore proceed as follows: Allow the spin system to evolve under all couplings in the Hamiltonian for a time τ_1 while the sample spins about an axis at angle θ_1, and then flip the axis to angle θ_2. At an evolution time $t_1 = \tau_1 + k\tau_1$ the anisotropic part of the interaction will refocus in an echo (*24*) corresponding to refocusing of the anisotropic frequencies. The amplitude at the point of echo formation evolves only under the isotropic frequency shifts due to chemical shielding ($\gamma\sigma_{\text{iso}}B_0$) and isotropic second-order quadrupolar ($\omega_{\text{iso}}^{(2)}$) interactions. Experiments are performed at a convenient set of angles (θ_1, θ_2) from Fig. 3 with division of the evolution time prescribed by the corresponding k value, that is, $\tau_2 = k\tau_1$.

As described in more detail in the following section, one may imagine performing variations of DAS as one- or two-dimensional experiments. In the one-dimensional case, the magnetization is sampled only at the echo maximum, where the amplitude evolves under the isotropic couplings as the evolution time is increased. In a two-dimensional experiment, there are two periods of evolution, t_1 and t_2, during which the spins evolve under two different Hamiltonians. A two-dimensional Fourier transformation produces a spectrum showing correlations of the frequencies in the two dimensions. In the DAS experiments described here the first time dimension is the high-resolution evolution under the isotropic shift terms only, while the second dimension encompasses the decay of the echo from the point of refocusing. This allows a correlation of the high-resolution isotropic resonances with the powder patterns obtained in variable-angle spinning experiments at the second spinning angle.

EXPERIMENTAL

Experiments were performed at 9.4 T corresponding to a sodium-23 resonance frequency of 105.84 MHz and an oxygen-17 resonance frequency of 54.24 MHz.

DAS probe. The flipping probehead (Fig. 5) was fabricated with Vespel, Delrin, and alumina parts, the choice of materials being dictated by their light weight, durability, and ease of machining as well as a history of performance in MAS applications (*17, 25*). An important feature of this design is that the coil is wrapped around the stator and is moved along with the spinning axis. This increases the filling factor compared to the alternative of a coil mounted externally to the stator body.

The stator body is coupled to a stepping motor at the base of the magnet with a Kevlar string, which is fastened to pulleys on the motor shaft and stator body and tightened with nylon turnbuckles. The motor is fully programmable, and a flip from $\theta_1 = 37.38°$ to $\theta_2 = 79.19°$ occurs in 36 ms. Instruction sets for the motor are stored in the motor controller, and the flipping is triggered by TTL-level pulses from the pulse programmer. With controller feedback from an encoder attached to the motor, precise movement during the hop and reproducible values of θ_1 and θ_2 for the experiment are accomplished.

An important element in these experiments is the control of the angles, and the best angular reference available spectroscopically is the magic angle, $\theta^{(2)}$, where

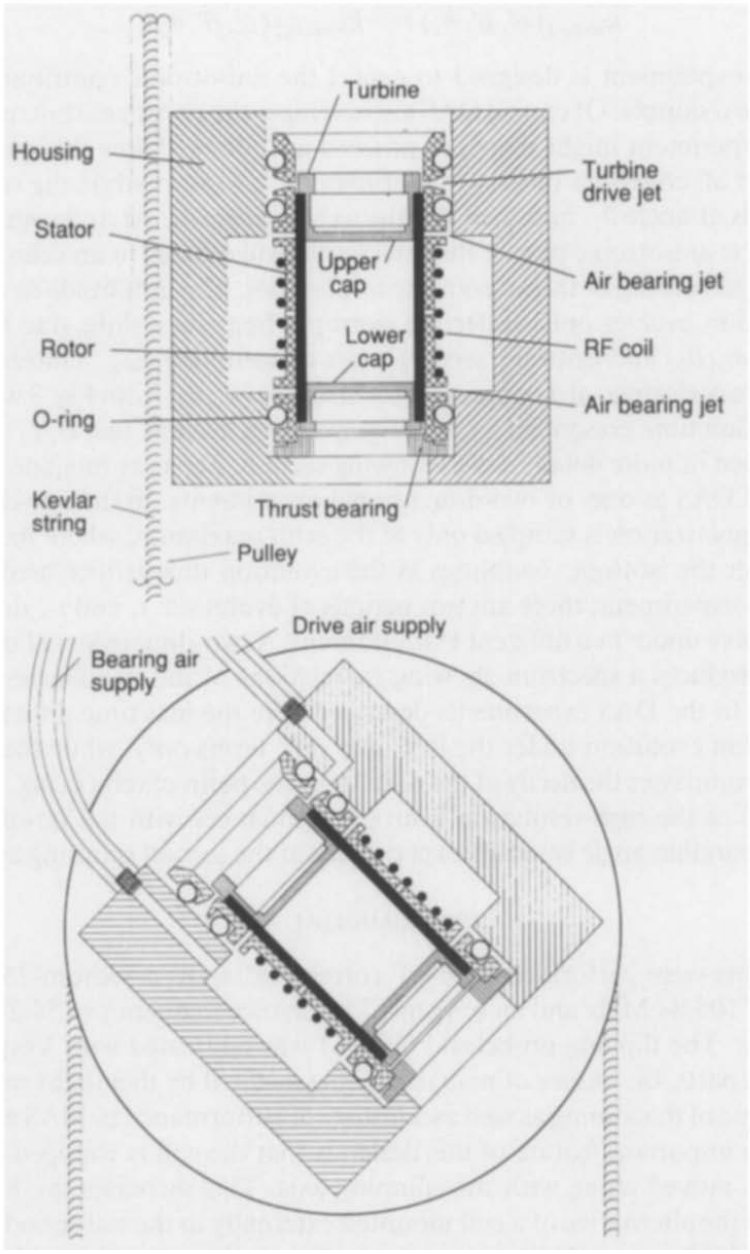

FIG. 5. Two cross-sectional views of the DAS probehead, illustrating the spinner mechanism, dual air-delivery systems, and mechanical axis flipping assembly.

$P_2(\cos\theta^{(2)}) = 0$. The magic angle was set in the sodium-23 experiments by maximizing the rotational echoes in a bromine-81 FID from solid KBr, which was packed in the sample spinner along with the powdered solids. The proximity of the bromine-81 resonance frequency to that of sodium-23 makes this a reasonable choice for an angular standard. For the oxygen-17 experiments the deuterium resonance in partially deuterated 1,4-dimethoxybenzene was used. After the spinning axis is set to the magic angle, the motor is moved to θ_1, and the number of steps necessary to reach θ_2

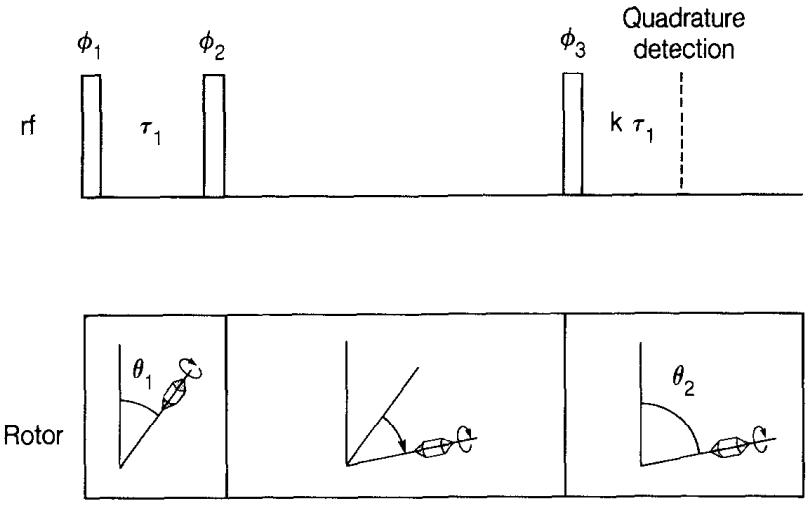

ϕ_1	ϕ_2	ϕ_3	Detection	
			Real	Imaginary
+x	+x	+x	+y	−x
+x	+x	−x	−y	+x
−x	+x	+x	−y	+x
−x	+x	−x	+y	−x
+y	+x	+x	−x	−y
+y	+x	−x	+x	+y
−y	+x	+x	+x	+y
−y	+x	−x	−x	−y

FIG. 6. Radiofrequency pulse sequence, rotor axis orientation relative to an external magnetic field along the z axis, and phase cycling used in the DAS experiments. All pulses are selective 90° pulses calibrated at the particular orientation angle.

is also calculated. Nominal motor resolution of 0.36° was obtained using a 1000 step incremental encoder and a 100 step motor with 1/16th of a step microstepping capability, leading to comparable angular resolution in the stator position due to a 1:1 pulley ratio.

Pulse sequence and phase cycling. Figure 6 shows the sequence of pulses and phases needed to perform the DAS experiments. All pulses are selective 90° pulses calibrated at both θ_1 and θ_2 on the central transition of the quadrupolar nuclei. For a spin I nucleus this should be $1/(I+\frac{1}{2})$ times the 90° pulse time for the full set of $|\Delta m| = 1$ transitions (*26*), i.e., that found in a nucleus with no quadrupolar coupling due to high crystal symmetry such as sodium-23 in solid NaCl. In the sodium-23 experiments the 90° pulse times were 6.2 μs at θ_1 and 4.1 μs at θ_2. Comparison of the 90° pulse time for a sample of solid NaCl to that of a quadrupolar sample verified the selective irradiation on the central transition of the quadrupolar nuclei. In the oxygen-17 experiments the 90° pulse times were approximately one-third of those in a sample of liquid $H_2{}^{17}O$, and were calibrated at 10.3 μs at θ_1 and 6.8 μs at θ_2.

TABLE 1

Time Development of the Reduced Density Matrix during a DAS Experiment in Each of the Eight Experiments of Fig. 6

Expt	$\rho(1^+)$	$\rho(\tau_1)$	ρ(storage)	$\rho(3^+)$	$\rho\,(t_1 = \tau_1 + \tau_2)$
1	$-I_y$	$-I_y\cos\omega_1\tau_1 + I_x\sin\omega_1\tau_1$	$-I_z\cos\omega_1\tau_1$	$+I_y\cos\omega_1\tau_1$	$+I_y\cos\omega_1\tau_1\cos\omega_2\tau_2 - I_x\cos\omega_1\tau_1\sin\omega_2\tau_2$
2	$-I_y$	$-I_y\cos\omega_1\tau_1 + I_x\sin\omega_1\tau_1$	$-I_z\cos\omega_1\tau_1$	$-I_y\cos\omega_1\tau_1$	$-I_y\cos\omega_1\tau_1\cos\omega_2\tau_2 + I_x\cos\omega_1\tau_1\sin\omega_2\tau_2$
3	$+I_y$	$+I_y\cos\omega_1\tau_1 - I_x\sin\omega_1\tau_1$	$+I_z\cos\omega_1\tau_1$	$-I_y\cos\omega_1\tau_1$	$-I_y\cos\omega_1\tau_1\cos\omega_2\tau_2 + I_x\cos\omega_1\tau_1\sin\omega_2\tau_2$
4	$+I_y$	$+I_y\cos\omega_1\tau_1 - I_x\sin\omega_1\tau_1$	$+I_z\cos\omega_1\tau_1$	$+I_y\cos\omega_1\tau_1$	$+I_y\cos\omega_1\tau_1\cos\omega_2\tau_2 - I_x\cos\omega_1\tau_1\sin\omega_2\tau_2$
5	$+I_x$	$+I_x\cos\omega_1\tau_1 + I_y\sin\omega_1\tau_1$	$+I_z\sin\omega_1\tau_1$	$-I_y\sin\omega_1\tau_1$	$-I_y\sin\omega_1\tau_1\cos\omega_2\tau_2 + I_x\sin\omega_1\tau_1\sin\omega_2\tau_2$
6	$+I_x$	$+I_x\cos\omega_1\tau_1 + I_y\sin\omega_1\tau_1$	$+I_z\sin\omega_1\tau_1$	$+I_y\sin\omega_1\tau_1$	$+I_y\sin\omega_1\tau_1\cos\omega_2\tau_2 - I_x\sin\omega_1\tau_1\sin\omega_2\tau_2$
7	$-I_x$	$-I_x\cos\omega_1\tau_1 - I_y\sin\omega_1\tau_1$	$-I_z\sin\omega_1\tau_1$	$+I_y\sin\omega_1\tau_1$	$+I_y\sin\omega_1\tau_1\cos\omega_2\tau_2 - I_x\sin\omega_1\tau_1\sin\omega_2\tau_2$
8	$-I_x$	$-I_x\cos\omega_1\tau_1 - I_y\sin\omega_1\tau_1$	$-I_z\sin\omega_1\tau_1$	$-I_y\sin\omega_1\tau_1$	$-I_y\sin\omega_1\tau_1\cos\omega_2\tau_2 + I_x\sin\omega_1\tau_1\sin\omega_2\tau_2$

Note. $\omega_i = \omega_{iso} + \sum_{\alpha',\beta'} \omega_{aniso}(\alpha', \beta', \theta_i)$; $\omega_{iso} = \gamma\sigma_{iso}B_0 + \omega_{iso}^{(2)}$ (see Eq. [6]). The equilibrium state before each sequence is $\rho(0) = I_z$, and the notation $\rho(n^+)$ signifies the density matrix immediately following the nth pulse.

To begin an experiment, the sample is set spinning at a frequency of approximately 3 kHz about an axis inclined at an angle θ_1 with respect to the external magnetic field. The first 90° pulse, with phase ϕ_1, brings the equilibrium magnetization from the central transition down into the xy plane where it evolves under chemical-shift and second-order quadrupolar interactions for a length of time τ_1. The second pulse with phase ϕ_2 stores a particular component of this evolved signal along the static magnetic field while the probe flips from θ_1 to θ_2.

Storage of the magnetization, as described by Maciel and co-workers (*16*) in their magic-angle hopping experiments, is necessary to quench the evolution of the magnetization during the axis flip. Since only one of the two orthogonal components of the magnetization in the xy plane may be stored during each flip, the quadrature data as a function of evolution time must be collected separately. Although only two experiments are needed to fully reconstruct the echo, we also phase cycle to cancel any residual xy magnetization after the third pulse. This makes it necessary to perform eight experiments for each value of the evolution time.

Following the axis flip, the stored magnetization component is returned to the xy plane with a pulse of phase ϕ_3 and, after a time $\tau_2 = k\tau_1$ determined by the choice of angles, a component of the full second-order flipped echo refocuses in the xy plane. At this time, one point may be accumulated with quadrature detection and added to the x and y data buffers according to the receiver (detection) phase. Calculating the resulting signal after the eight phase-cycled experiments, it is found that the magnetization as a function of $t_1 = \tau_1 + \tau_2$ indeed yields a second-order quadrupolar echo. Tables 1 and 2 supply the details of the calculation.

Experiments are performed in either of two ways: (1) as one-dimensional experiments with the digitization of only the points at the refocusing of each echo as a function of the evolution time or (2) as two-dimensional experiments with incrementation of the evolution time $t_1 = \tau_1 + \tau_2$ for the first dimension and accumulation of

TABLE 2

The Magnetization Measured in Each of the Eight Experiments of Fig. 6

Expt	x buffer	y buffer
1	$+\cos\omega_1\tau_1\cos\omega_2\tau_2$	$+\cos\omega_1\tau_1\sin\omega_2\tau_2$
2	$+\cos\omega_1\tau_1\cos\omega_2\tau_2$	$+\cos\omega_1\tau_1\sin\omega_2\tau_2$
3	$+\cos\omega_1\tau_1\cos\omega_2\tau_2$	$+\cos\omega_1\tau_1\sin\omega_2\tau_2$
4	$+\cos\omega_1\tau_1\cos\omega_2\tau_2$	$+\cos\omega_1\tau_1\sin\omega_2\tau_2$
5	$-\sin\omega_1\tau_1\sin\omega_2\tau_2$	$+\sin\omega_1\tau_1\cos\omega_2\tau_2$
6	$-\sin\omega_1\tau_1\sin\omega_2\tau_2$	$+\sin\omega_1\tau_1\cos\omega_2\tau_2$
7	$-\sin\omega_1\tau_1\sin\omega_2\tau_2$	$+\sin\omega_1\tau_1\cos\omega_2\tau_2$
8	$-\sin\omega_1\tau_1\sin\omega_2\tau_2$	$+\sin\omega_1\tau_1\cos\omega_2\tau_2$
Sum	$4\cos(\omega_1\tau_1+\omega_2\tau_2)$	$4\sin(\omega_1\tau_1+\omega_2\tau_2)$

Note. The relative phase for addition to the data buffers is chosen by the detector (receiver) phase in the pulse program. Note that $\omega_1\tau_1 + \omega_2\tau_2 = \omega_{iso}t_1$ (see Eq. [13]) resulting in a second-order quadrupolar echo whose maximum evolves at the isotropic frequency only.

the full FID following the echo maximum at t_2. Examples of each of these approaches will be presented. In case (2), two-dimensional correlation spectra are obtained where the F_1 dimension reveals the isotropic shift observed for each of the second-order lineshapes at θ_2 appearing in the F_2 dimension.

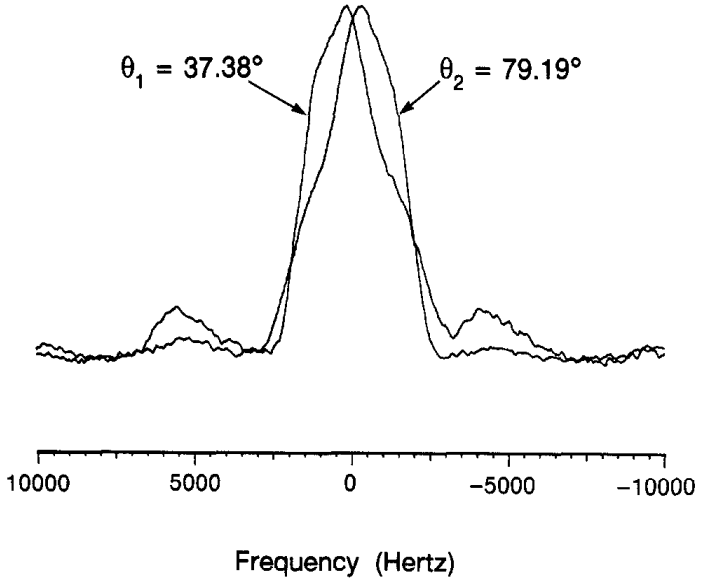

FIG. 7. Superimposed sodium-23 spectra of $Na_2C_2O_4$ with sample spinning at the two angles used in the DAS experiment with $k = 1$. The zero on the frequency scale is the point of intersection of these two spectra and corresponds to the experimentally determined isotropic shift frequency from the DAS experiments. The spinning speed in each is 4.5 kHz.

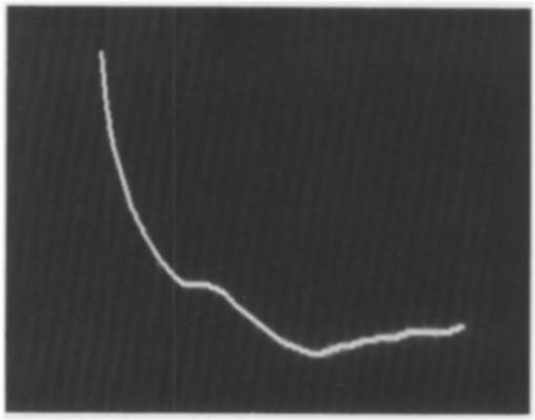

(a) FID

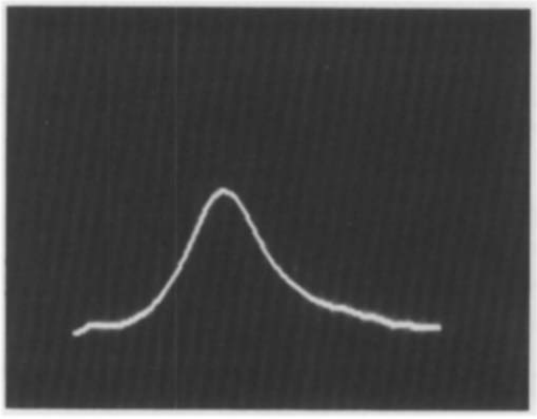

(b) Echo

FIG. 8. (a) The free induction decay of the magnetization in the central transition of Na_2SO_4, which begins directly after a 90° pulse, decays in time during the 640 μs scan shown. (b) Second-order quadrupolar echo of transverse magnetization in the flipped axis experiments of Fig. 6, reconstructed from the eight experiments as explained in Tables 1 and 2. The time scale is the same as in (a), but begins 180 μs before the echo maximum, which occurs at $t_1 = 1$ ms.

RESULTS

Spinning around a fixed axis. The static powder pattern and MAS spectrum of sodium-23 in $Na_2C_2O_4$ were shown in Fig. 2. In Fig. 7, spectra from samples spinning at complementary angles $\theta_1 = 37.38°$ and $\theta_2 = 79.19°$ display the reflection symmetry expected from Eqs. [11]–[13], and the simulations of Fig. 4. This is a convenient set of complementary angles for a DAS experiment, since $k = 1$ and the two evolution periods leading to the echo are equal. At these angles there is additional broadening of the specta due to homonuclear dipole–dipole interactions and chemical-shift anisotropy.

Second-order quadrupolar echo. Consider the experiment illustrated in Fig. 6 with a sample of polycrystalline sodium sulfate (Na_2SO_4; $e^2qQ/h = 2.6$ MHz, $\eta = 0.6$),

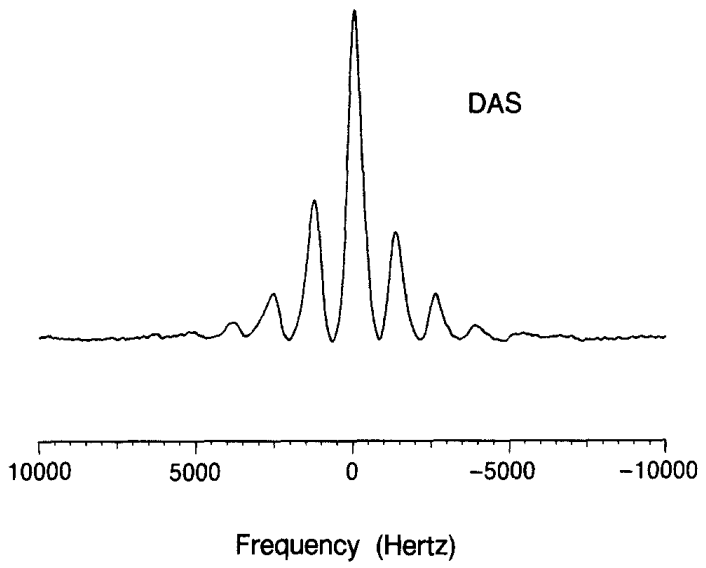

FIG. 9. One-dimensional DAS spectrum of $Na_2C_2O_4$. The eight-part experiment of Fig. 6 was repeated four times for each of 256 points in t_1, with a Δt of 8 μs, resulting in a spectral width of 62.5 kHz. The scale has been expanded to 20 kHz, and sidebands occur at half of the rotor frequency, as explained in the text.

an axis flip from $\theta_1 = 37.38°$ to $\theta_2 = 79.19°$, and evolution times $\tau_1 = \tau_2 = 500$ μs. After the first pulse, while the sample is spinning at θ_1, the magnetization evolves at the frequencies in the θ_1 spectrum of Fig. 7. An oscilloscope trace of the decay of the signal is shown in Fig. 8a. After 500 μs, a second pulse is applied to store a component of the magnetization. After the flip to θ_2, another pulse restores this component of the magnetization, which now evolves under the influence of the frequencies of the θ_2 spectrum in Fig. 7. The result is that the anisotropic frequencies cancel, and a full echo may be reconstructed after eight experiments, as shown in Fig. 8b. At the echo maximum, centered at $t_1 = \tau_1 + \tau_2$, only the isotropic frequency evolution remains. The echoes indicate the refocusing of first-order effects (e.g., chemical-shift anisotropy) and second-order quadrupolar broadening. Due to spin diffusion during the storage of magnetization components, the dipole–dipole couplings are not completely refocused and this limits the resolution in DAS experiments. Thus DAS is likely to be most applicable to dilute spins.

Sodium-23 DAS results. The DAS experiment with $k = 1$ is performed with a set of evolution periods t_1, incremented by simultaneously changing τ_1 and τ_2 by a short time Δt, on the order of 10 to 100 μs. The effective bandwidth in the high-resolution spectrum is $1/2\Delta t$. Sodium-23 results have been obtained on both $Na_2C_2O_4$ and Na_2SO_4, and they are presented here in the form of one- and two-dimensional experiments to illustrate the information content of each.

In $Na_2C_2O_4$, the echo amplitudes were digitized in quadrature and the resulting FID in t_1 was Fourier transformed to produce the one-dimensional spectrum of Fig. 9. This high-resolution spectrum contains one isotropic line, shown at 0 Hz on the frequency axis, with a linewidth of 575 Hz. The sideband pattern has a spacing of 1.5 kHz, which is one-half of the rotational frequency of the rotor. The appearance of

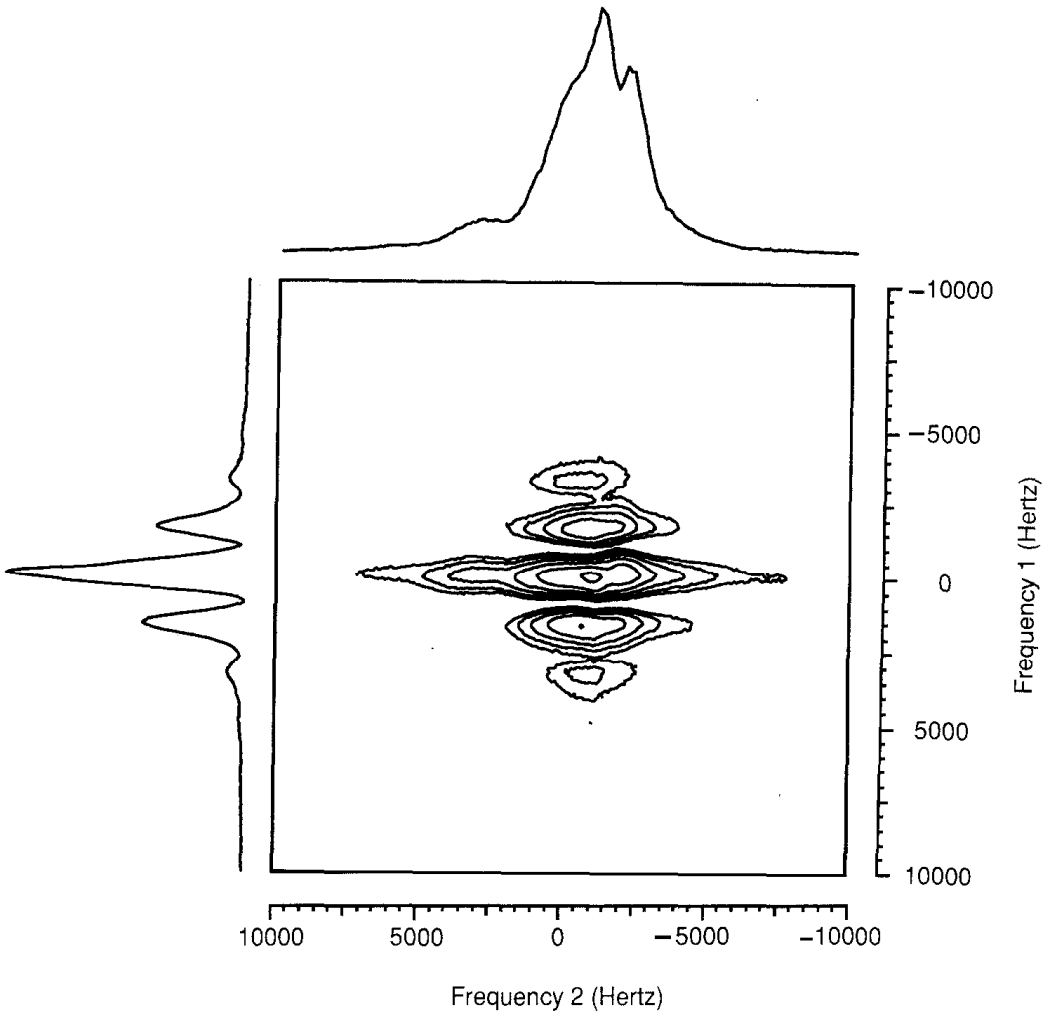

FIG. 10. Two-dimensional DAS spectrum of Na_2SO_4 correlating the isotropic shift obtained in the first frequency dimension (horizontal) with the lineshape observed in the second dimension while spinning at an angle of 79.19°. The off-angle spectrum matches that of the simulations with $\eta = 0.6$.

sidebands at half of the rotation frequency is expected since the evolution is divided into two periods with a storage of the magnetization between them. This effect is similar to that seen in two-dimensional spin-echo experiments (*27*).

The spectrum is narrowed by a factor of seven from the MAS results, and the isotropic frequency is easily identified from the maximum of the symmetric central peak. The oxalate spectra previously shown (Figs. 2 and 7) have been placed on an isotropic frequency axis, with the zero point placed at this experimentally determined value.

A two-dimensional DAS power spectrum for sodium-23 in polycrystalline Na_2SO_4 is presented in Fig. 10. The data were taken as a series of complex FIDs in two dimensions. The t_1 domain is the sum of the evolution times at the two angles ($t_1 = \tau_1 + \tau_2$), which was incremented by $2\Delta t = 20$ μs for each t_1 point. The second time domain

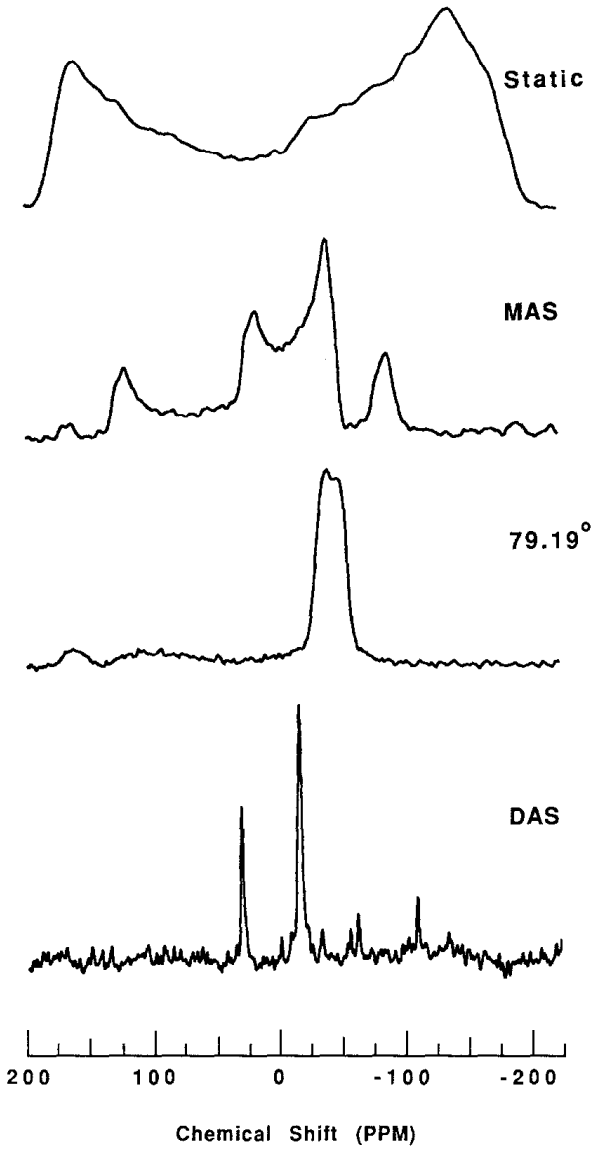

FIG. 11. The oxygen-17 static, MAS, variable-angle spinning (at 79.19°), and one-dimensional DAS spectra for cristobalite. The single oxygen isotropic shift is at −16.6 ppm with respect to $H_2{}^{17}O$.

(t_2) is the decay of the echo after the refocusing. The F_2 projection, corresponding to the spectrum of the FIDs, is the spectrum from the sample spinning with the axis at 79.19° as expected. In the F_1 dimension, a narrowed line at the isotropic shift is found, along with spinning sidebands. Spectral resolution is determined by sodium–sodium dipolar coupling.

Oxygen-17 DAS results. For oxygen-17, narrower lines are expected, due to weaker dipolar interactions. Application of DAS is demonstrated in Fig. 11 for the mineral cristobalite (SiO_2), enriched to 37% in oxygen-17. The quadrupolar parameters for the one distinct oxygen site are $e^2qQ/h = 5.8$ Mhz and $\eta = 0$. The isotropic shift has been referenced as shifted by −16.6 ppm from the oxygen-17 resonance in $H_2{}^{17}O$.

The isotropic peak is determined by performing the experiment at two different spinning speeds.

Comparison to the static, MAS and 79.19° spinning spectra emphasize the information content and resolution enhancement possible with these experiments. The linewidth in the DAS spectrum is approximately 200 Hz, while the MAS spectrum is difficult to characterize due to the slow spinning speed with respect to the strong quadrupolar interaction. The off-angle spinning spectrum points out the utility of spinning at an angle other than the magic angle, but the isotropic shift may not be directly determined from a peak in the spectrum.

CONCLUSIONS

Flipping the spinning axis, combined with RF pulsing and storage of the magnetization, comprises a new family of experiments which provide narrowing of NMR resonances broadened by second-order interactions. Resonances in the high-resolution dimension are obtained at the sum of the isotropic chemical and isotropic second-order quadrupolar shifts. While, in the sodium-23 systems studied, dipolar interactions result in a further broadening of the spectral lines, a gain in resolution up to seven times that found in MAS experiments has been recorded. Both one- and two-dimensional experiments have been demonstrated, with the second dimension providing a correlation of isotropic shifts to the second-order broadened patterns obtained while spinning at the second angle in the experiment. For oxygen-17, resolution of 200 Hz has been obtained in a system with a large second-order quadrupolar broadening. A sideband pattern is obtained with a spacing of one-half of the rotor frequency since the spinning frequency is much less than the interaction strength.

The new techniques designed to remove second-order broadening should also be useful approaches to problems involving other second-order effects. Particularly interesting are second-order dipole–dipole (*28*), magnetic susceptibility (*29*), and dipole–quadrupole (*30*) interactions. It is also anticipated that with a combination of synchronized DAS and multiple-pulse experiments it should be possible to perform an experiment analogous to those of Tycko (*31, 32*) in which the truncation induced by the large external magnetic field is undone. An advantage of these applications compared to the continuous rotations (DOR) is that more complex trajectories designed to average higher-order interactions should be possible.

ACKNOWLEDGMENTS

We thank C. J. Lee and A. Samoson for helpful discussions, and B. F. Chmelka and J. Stebbins for preparation of oxygen-17 compounds. The probehead was built by H. Graetsch and C. Gaskins in the College of Chemistry machine shop. K.T.M. is an N. S. F. Graduate Fellow. This work was supported by the Director, Office of Energy Research, Office of Basic Energy Sciences, Materials Science Division of the U. S. Department of Energy under Contract DE-AC03-76SF00098.

REFERENCES

1. E. R. ANDREW, A. BRADBURY, AND R. G. EADES, *Nature (London)* **182,** 1659 (1958).
2. I. J. LOWE, *Phys. Rev. Lett.* **2,** 285 (1959).
3. J. SCHAEFER AND E. O. STEJSKAL, *J. Am. Chem. Soc.* **98,** 1031 (1976).

4. C. A. FYFE, "Solid State NMR for Chemists," CFC Press, Guelph, 1983.
5. M. MUNOWITZ, "Coherence and NMR," Wiley, New York, 1988.
6. U. HAEBERLEN AND J. S. WAUGH, *Phys. Rev.* **175,** 453 (1968).
7. R. V. POUND, *Phys. Rev.* **79,** 685 (1950).
8. M. H. COHEN AND F. REIF, *Solid State Phys.* **5,** 321 (1957).
9. S. SCHRAMM AND E. OLDFIELD, *J. Am. Chem. Soc.* **106,** 2502 (1984).
10. A. SAMOSON, E. KUNDLA, AND E. LIPPMAA, *J. Magn. Reson.* **49,** 350 (1982).
11. S. GANAPATHY, S. SCHRAMM, AND E. OLDFIELD, *J. Chem. Phys.* **77,** 4360 (1982).
12. G. E. MACIEL, *Science* **226,** 282 (1984).
13. A. LLOR AND J. VIRLET, *Chem. Phys. Lett.* **152,** 248 (1988).
14. A. SAMOSON, E. LIPPMAA, AND A. PINES, *Mol. Phys.* **65,** 1013 (1988).
15. G. C. CHINGAS, C. J. LEE, E. LIPPMAA, K. T. MUELLER, A. PINES, A. SAMOSON, B. Q. SUN, D. SUTER, AND T. TERAO, *in* "Proceedings, XXIV Congress Ampère, Poznań, 1988" (J. Stankowski, N. Piślewski, and S. Idziak, Eds.), D62, 1988.
16. A. BAX, N. M. SZEJVERENYI, AND G. E. MACIEL, *J. Magn. Reson.* **52,** 147 (1983).
17. T. TERAO, H. MIURA, AND A. SAIKA, *J. Chem. Phys.* **85,** 3816 (1986).
18. B. F. CHMELKA, K. T. MUELLER, A. PINES, J. STEBBINS, Y. WU, AND J. W. ZWANZIGER, *Nature (London)* **339,** 42 (1989).
19. U. HAEBERLEN, *in* "Advances in Magnetic Resonance" (J. S. Waugh, Ed.), Suppl. 1, Academic Press, New York, 1976.
20. M. MEHRING, "Principles of High Resolution NMR in Solids," 2nd ed., Springer-Verlag, New York, 1983.
21. K. NARITA, J. UMEDA, AND H. KASUMOTO, *J. Chem. Phys.* **44,** 2719 (1966).
22. C. J. LEE, Ph.D. thesis, University of California, Berkeley, 1987.
23. C. J. LEE, A. SAMOSON, B. Q. SUN, T. TERAO, AND A. PINES, *Proc. Natl. Acad. Sci. USA,* to be published.
24. E. L. HAHN, *Phys. Rev.* **80,** 580 (1950).
25. F. D. DOTY AND P. D. ELLIS, *Rev. Sci. Instrum.* **52,** 1868 (1981).
26. V. H. SCHMIDT, *Phys. Rev. B* **7,** 4145 (1973).
27. G. BODENHAUSEN, S. P. KEMPSELL, R. FREEMAN, AND H. D. W. HILL *J. Magn. Reson.* **35,** 337 (1979).
28. D. L. VANDERHART, *J. Chem. Phys.* **84,** 1196 (1986).
29. D. L. VANDERHART, W. L. EARL, AND A. N. GARROWAY, *J. Magn. Reson.* **44,** 361 (1981).
30. E. KUNDLA AND M. ALLA, *in* "Proceedings, XX Congress Ampère, Tallinn, 1978" (E. I. Kundla, E. Lippmaa, and T. Saluvere, Eds.), p. 92, 1979.
31. R. TYCKO, *J. Magn. Reson.* **75,** 193 (1987).
32. R. TYCKO, *Phys. Rev. Lett.* **60,** 2734 (1988).